Mobile Small Polarons Qualitatively Explain Conductivity in Lithium Titanium Oxide Battery Electrodes

Matthias Kick,[†] Cristina Grosu,[†,‡] Markus Schuderer,[†] Christoph Scheurer,[†] and Harald Oberhofer[*,†]

[†]*Chair for Theoretical Chemistry and Catalysis Research Center, Technical University of Munich, Lichtenbergstr. 4, 85747 Garching, Germany*

[‡]*Institute of Energy an Climate Research (IEK-9), Forschungszentrum Jülich, 52425 Jülich, Germany*

E-mail: harald.oberhofer@tum.de

Abstract

Lithium titanium oxide $Li_4Ti_5O_{12}$ (LTO) is an intriguing anode material promising particularly long lived batteries, due to its remarkable phase stability during (dis)charging of the cell. However, its usage is limited by its low intrinsic electronic conductivity. Introducing oxygen vacancies can be one method to overcome this drawback, possibly by altering the charge carrier transport mechanism. We use Hubbard corrected density-functional theory (DFT+U) to show that polaronic states in combination with a possible hopping mechanism can play a crucial role in the experimentally observed increase of electronic conductivity. To gauge polaronic charge mobility, we compute relative stabilities of different localization patterns and estimate polaron hopping barrier heights.

Introduction

Energy storage solutions such as Li-ion batteries (LIB) are a key technology in the transition from a fossil fuel based economy to a society based on sustainable resource management.[1,2] Despite the tremendous advancements in battery research over the last few years,[3] durability and especially storage capacity still need significant improvements for batteries to represent a viable alternative e.g. in the transport and mobility sectors.[2,4] One promising material envisioned as a potential remedy for these problems in conventional as well as all-solid state batteries (ASSB) is lithium titanium oxide (LTO).[2] Zero strain insertion, high cycling stability and a stable charge/discharge plateau render LTO an excellent anode material for long living batteries.[2,4–6] Its general use, however, is still limited by the fact that LTO suffers from a very low intrinsic electronic conductivity.[7,8] One way to overcome this drawback is to expose LTO to a reductive hydrogen atmosphere at elevated temperatures, leading to the formation of oxygen vacancies. As experimental data shows,[9] this not only causes a color change from white to blue but also lowers electronic resistance and impedance. Moreover, this blue LTO also shows improved Li-ion mobility compared to pristine white LTO.[9]

Unfortunately, neither of these improvements in carrier mobility are currently fully understood from a mechanistic viewpoint. Yet, first hints at the nature of the improved electronic conductivity in LTO emerged recently with the experimental discovery of paramagnetic Ti^{3+} centers.[8–11] Furthermore, calculations on doped LTO[12] and experimental data[13] seem to indicate that electron hopping between adjacent Ti centers is responsible for the increase of electronic conduction. However, earlier theoretical results were based on standard semi-local density functional theory (DFT) and thus suffered from sizeable self-interaction errors (SIE).[14] Therefore, they were unable to represent either the alignment of defect-induced states with regards to the conduction band or the correct localization of these states as Ti^{3+} centers. It is by now well known[15,16] that a correct treatment of such charge-localized, polaronic states needs to rely on methods that at least partly mitigate the SIE.

The significance of Ti^{3+} centers becomes apparent considering an analogous case in TiO_2,

where oxygen vacancies are known to lead to the formation of small polarons mainly localized on Ti sites.[15–17] Further, experimental data also indicates polaronic transport in $Li_7Ti_5O_{12}$.[18] While polarons in TiO_2 are somewhat attracted to the vacancy itself,[19,20] they were also shown to be very mobile, with kinetic barriers that can easily be overcome at room temperature.[21] In this context we studied the formation and stability of polarons in bulk LTO, as well as the kinetic barriers separating them.

Results

For our analysis we considered a $2 \times 2 \times 1$ supercell of $Li_{32}Ti_{40}O_{96}$ (LTO) in its most stable[6] spinel configuration,[22] and created an oxygen vacancy at the energetically most favorable of the symmetry inequivalent sites (cf. supplementary material). This realization of the structural Li/Ti disorder is known to exhibit a Ti-deficient zone separating titanium layers as illustrated in Figure 1. It therefore lets us examine the interplay between structure, in the form of Li-rich and Li-poor regions, and function of the material. Removing a neutral oxygen atom from the simulation cell gives rise to two excess electrons, which can form two polaronic Ti^{3+} centers. Our simulation cell thus contains a oxygen defect concentration of 1.04 at%, well within the experimental range of up to 6 at%.[13] In standard semi-local LDA[23] or GGA[24] based DFT these can generally not be described at all due to the functionals' well known charge and spin delocalization errors.[25] As a cost-efficient remedy, we here make use of the popular Hubbard corrected[26–28] variant of the PBE[24] functional (PBE+U) in combination with the matrix control approach.[29,30] This combination has not only been shown to give easy access to all manners of polaron configurations but also to yield excellent results compared to the computationally much more expensive hybrid DFT functionals.[19] From a methodological point of view, a key aspect of DFT+U is the choice of the correct projector-dependent Hubbard U value.[19,31] A common strategy would be to choose the value according to the experimentally determined defect position within the band gap.[15,19] However, owing to the

relative novelty of blue LTO, there are no such results to be found in the literature. On the other hand, for TiO_2 the gap state position is experimentally known to be about 1 eV below the conduction band minimum (CBM)[32]. Arguably, titanium atoms in both LTO an TiO_2 are embedded in a similar chemical environments, leading to similar positions of the defect state within the band gap. This assumption is further supported by the observation that both defective TiO_2 and LTO show the same blue color.[9,13,33] Based on this approximation, all our further analyses are conducted with a U value of 2.65 eV, yielding gap states at around 1 eV below the CBM for the most stable polaronic configurations found. This value of U is further supported by the fact that hybrid DFT calculations with the popular HSE06[34] functional reproduce the observed level alignments (1.18 eV below the CBM for the most stable polaronic configuration).

Given the great structural complexity of defect-rich LTO, there is a large number—$\binom{40}{2} = 780$—of unique polaron localization patterns even in our relatively small simulation box. To distinguish them we calculated their relative stability according to $E_{\mathrm{rel}} = E_{\mathrm{tot,i}} - E_{\mathrm{tot,\,min}}$, where $E_{\mathrm{tot,i}}$ denotes the total energy of a given simulation box calculated with DFT and $E_{\mathrm{tot,\,min}}$ denotes the total energy of the most stable structure found so far. Hence, following standard procedures,[15] the most stable configuration serves as zero point of our energy scale, with all other configurations possessing positive relative energy.

An exhaustive computational sampling is complicated further by the fact that the electrons can localize both in a triplet or an open-shell singlet configuration.[15,16] On the other hand, many of these patterns are, if not fully degenerate, at least very close in energy. For a first demonstration of the existence and mobility of polarons in LTO and their influence on the electronic conductivity a complete sampling of all configurations is therefore not necessary. Instead, we focus on triplet configurations and localization patterns representative for the system as a whole. In detail, we considered 13 patterns with different distances to the defect site, localized within different Ti layers in the bulk unit cell. To distinguish them, we adapt a naming convention used in our earlier work[19] to the case of LTO, cf. Fig-

ure 1. We found the most stable defect position to be located in the center of the Ti-rich region of our layered LTO model (black circle in Figure 1, cf. also supplementary material). This localization is not at all surprising, as it allows the O-vacancy to be as far as possible from the Li-rich zone of our simulation cell and the structural distortions caused by it. Using this defect position throughout, Table 1 lists our obtained results regarding the relative stability of different polaron localization patterns. We found that the most stable

Table 1: Relative stabilities of the most representative polaronic configurations. The systems are ordered by their relative stabilities. A complete list of calculated systems can be found in the supplementary information. Also shown is the shortest periodic distance between the two Ti^{3+} centers ($d_{Ti^{3+}-Ti^{3+}}$).

For vertical layer–layer distances see Fig. 1.

system	E_{rel} [eV]	$d_{Ti^{3+}-Ti^{3+}}$ [Å]	system	E_{rel} [eV]	$d_{Ti^{3+}-Ti^{3+}}$ [Å]
L3-7/L2-9	0.00	6.6	L5-1/L3-12	0.45	7.9
L3-8/L3-4	0.12	6.0	L4-2/L4-4	0.75	5.9
L3-7/L3-12	0.13	7.9	L1-1/L1-4	0.77	10.0
L2-7/L2-8	0.14	5.9	L5-5/L4-2	0.82	7.9
L3-9/L3-12	0.23	3.0	L4-3/L4-4	1.00	6.0
L2-9/L2-12	0.26	2.9	L5-1/L5-5	2.59	6.0

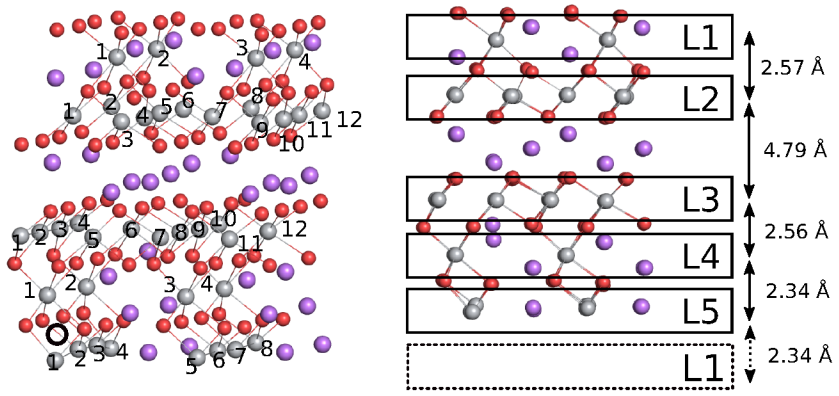

Figure 1: Sketch of the site naming convention of the different localization patterns. Lx-m/Ly-n specifies the localization of one electron within layer Lx on atom m with the second electron localized in layer Ly on atom n. Additionally, the position of the oxygen vacancies is marked with a black circle. Titanium atoms are depicted as grey spheres, oxygen atoms are shown as red spheres. On the right, arrows and numbers indicate the average inter layer titanium distance within the given unit cell.

configurations are those where one polaron is located in L2 and the other is located in L3

(cf. Figure 3a), followed by configurations where both polarons are either located in L2 or L3. The main difference is that "same-plane" polarons approach each other more closely and hence Coulomb repulsion is more pronounced compared to the most stable L3-X/L2-Y configurations. Furthermore, our analysis shows that there is also a tendency for polarons to be less stable the closer they are located to the defect site. This is clearly indicated by the configurations where both excess electrons are localized on Ti atoms belonging to layers L4 or L5 (see supplementary information for detailed distances to the defect site). Both of these effects compete with each other, such that polarons try to adopt configurations with maximal distances to the defect and between each other. This situation seems similar to TiO_2 where the oxygen defect is acting as a charge trapping center.[33,35] However, in LTO one can not directly extract a clear stability trend with the distance to the defect, as positively charged Li-ions also show some influence on the overall stabilities of the polarons.[36] Indeed, our choice of LTO cell allows us to quantify their influence, considering the fact that all our most stable defect configurations are located next to the Li-rich zone situated between L2 and L3.

Indeed, as Figure 2 shows we observe the formation of mid-gap defect states in contrast to earlier work by Tsai *et al.*[12] and Nasara *et al.*[13] where simple semi-local DFT led to a coalescence of the defect sates with the CBM. It is important to note, though, that the relative polaron stabilities are directly linked to the gap state position. In other words, polaronic configurations which are less stable have gap states lying higher in energy, closer to the CBM. Yet, this means that the absolute stabilities of the observed polarons depend on the choice of the U value used in the Hubbard correction. On the other hand, relative stability trends between polarons were shown to be largely unaffected for a reasonable range of U values (cf. supplementary material), reproducing results found e.g. for TiO_2[15].

Finally, in order to gauge the polaron mobility we calculate hopping barriers between our most stable configuration and adjacent Ti atoms. To this end, we again make use of the matrix control approach,[29,30] but with a modified occupation matrix scheme outlined in the

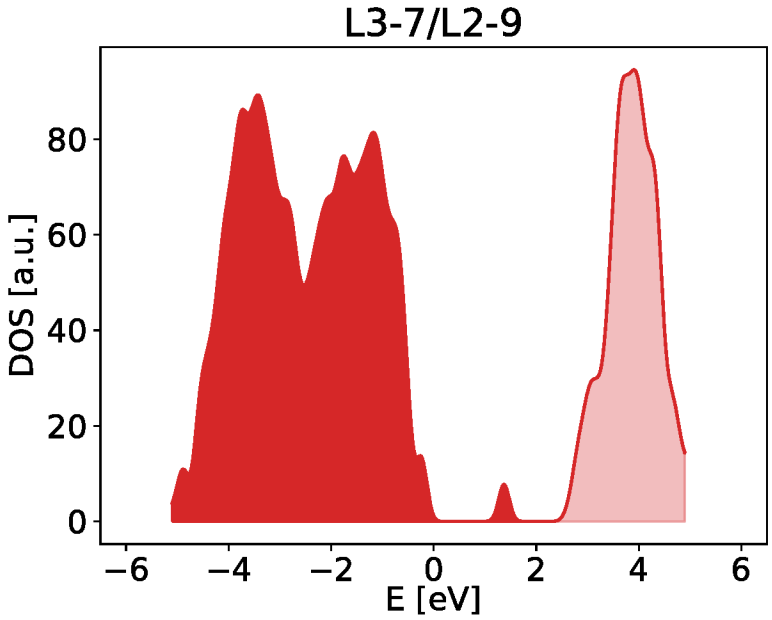

Figure 2: Representative for the found polaronic configurations we show the spin up density of states (DOS) of the most stable configuration L3-7/L2-9. Darker shading signifies occupied states, while lighter hues are unoccupied. The gap states—which have almost the same energy—appear about one 1 eV below the CBM. The valence band edge (VBM) serves as the zero point of the energy scale.

supplementary material. This approach allows us to restrain the electronic configuration of the system along a pre-selected reaction coordinate x, which linearly interpolates between two stable polaronic states, localized at neighboring atoms. Representatively for all hopping processes in the system we compute the "in-plane" transition of L3-7/L2-10 (x = 0.0) to L3-7/L2-9 (x = 1.0) and the "out-of-plane" transition of L3-7/L1-3 (x = 0.0) to L3-7/L2-9 (x = 1.0).

We illustrate this pathway in Figure 3, which in a) shows the spin density of the final state L3-7/L2-9 and in b) depicts we the relaxation of atoms from their respective sites in the pristine crystal for the transition from L3-7/L2-10 to L3-7/L2-9 via a transition state. We thereby only depict O atoms nearest to the involved Ti sites as only these show any significant distortion during a full geometry optimization. Figure 3b clearly shows relaxation of the O-atoms towards the respective Ti^{3+} sites in the initial (L2-10, blue) and final (L2-9, red) states, indicating a small polaron hopping mechanism. A similar picture arises for the transition from L3-7/L1-3 to L3-7/L2-9 (not pictured).

The energy profiles of these two transitions are depicted in Figure 4. As highlighted by the dashed black lines, the hopping barriers for transition L3-7/L2-10 to L3-7/L2-9 and for transition L3-7/L1-3 to L3-7/L2-9 are 186 meV and 583 meV respectively, with the later being much larger due to the already significant energy difference of 485 meV between the two stable states. With these barrier heights we can roughly estimate the in- and out-of-plane conductivity based on a simple hopping model assuming an Arrhenius-like thermal activation (cf. supplementary material).[37–39] Additionally, we are using an experimentally determined density of Ti^{3+} centers of 13.1 at%[13] as a measure for the charge carrier density. For the in-plane conductivity we thus find a value of 95.3 mS/cm, while the significantly higher out-of-plane hopping barrier results in a much smaller conductivity of 17×10^{-6} mS/cm. To put these results into context, even our lower bound for the conductivity of reduced LTO is already five orders of magnitude higher than the pristine material,[13] while our ideal upper bound is of the order of the ion conductivities in currently employed electrolytes.[40]

The literature for reduced LTO shows experimentally measured electronic conductivities in the range of 10^{-2} to 5×10^{-2} mS/cm[18,41], which compare reasonably well with our rough estimates for an idealized system. Note that the estimate for the ideal conductivity rests on the assumption that there are no other, significantly higher barriers along the whole pathway of charge percolation through the crystal. This implies a distribution of defects aligned along the [100] axis of the crystal. Considering the fairly high density of oxygen defects present in blue LTO, such a case is certainly achievable. Finally, it should be noted that in our model pristine LTO would show a conductivity of exactly zero due to a complete lack of any free charge carriers.

Discussion

To conclude, our stability analysis clearly indicates that the experimentally observed Ti^{3+} centers in reduced LTO can in fact be the result of small polaron formation. Moreover, comparatively small barrier heights indicate that charge hopping dynamics can already occur at room temperature. This renders a polaron hopping mechanism to be the most likely origin of the increased electronic conductivity observed in blue LTO. Indeed a simple conductivity model puts even the worst estimate of 17×10^{-6} mS/cm five orders of magnitude above pristine LTO. On the other hand, the ideal predicted case based on an in-plane hopping mechanism would lead to a conductivity of 100 mS/cm, which, though significantly lower than that of other anode materials,[40,42,43] is nevertheless comparable to the ion conductivities of the pristine material and super–ionic conductors.[2,10,44] Moreover, the existence of polarons also hints at a mechanism for the improved ion diffusivity in blue LTO, which is about twice that of pristine LTO.[13] The presence of polarons, which we have shown to localize near Li-rich regions, could serve to "soften" the environment for Li-diffusion by screening the positive charge carriers. Thus, both, the ideal polaron conductivity of blue LTO, and its improved Li diffusivity, would make it a suitable option for an anode material for use in

tomorrow's batteries. Note that our results show a very wide range of potential conductivity values, depending on defect patterning, local crystal structure and crystal orientation. Our study thus highlights the potential and also pitfalls of defect engineering as a means for the generation of mobile charge carriers in otherwise insulating materials.

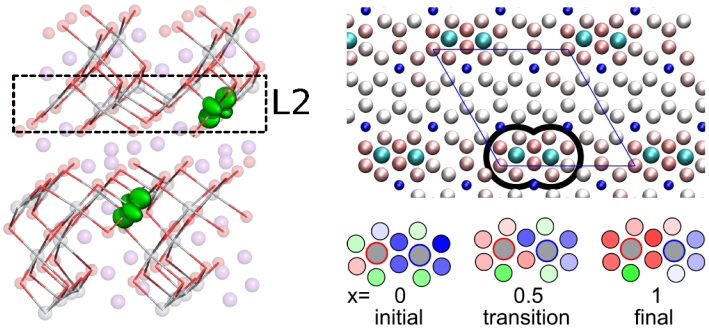

Figure 3: a) Spin density of the most stable configuration L3-7/L2-9 of our simulation. Isosurface level 0.015 eÅ^{-3}. b) Top: cut through the simulation cell showing the L2-layer, showing the distortion of the lattice at the transition state. Atoms in cyan indicating the L2-9 and L2-10 positions respectively. Darker red colors indicate a stronger movement during the transition from L3-7/L2-10 to L3-7/L2-9. Note that only nearest neighbor oxygen atoms show significant movement, indicating indeed the hopping of a small polaron. Bottom: schematic of the movement of oxygen atoms from their undistorted sites for the transition from L3-7/L2-10 (left) to L3-7/L2-9 (right) via a transition state (center). Circles filled in red hues indicate a predominant movement of the respective O atom towards the Ti atom at L2-9 (red circle filled with grey), while blue hues depict a movement towards L2-10 (blue circle filled with grey). Circles filled in green hues show movement not clearly aimed at either Ti atoms. In all cases darker colors indicate stronger movement.

Methods

All necessary calculations have been carried out using the FHI-aims code.[45] To achieve adequate electron localization we used the DFT+U[27] variant of the PBE[24] exchange correlation functional. In detail we used the rotationally invariant +U form[28] with the double-counting correction in the fully localized limit.[31] The Ti 3*d* atomic like basis functions served as Hubbard projectors and a U value of 2.65 eV has been applied. Numerical convergence has been reached using a *tight tier1* basis—roughly equivalent to a polarized triple zeta split valence

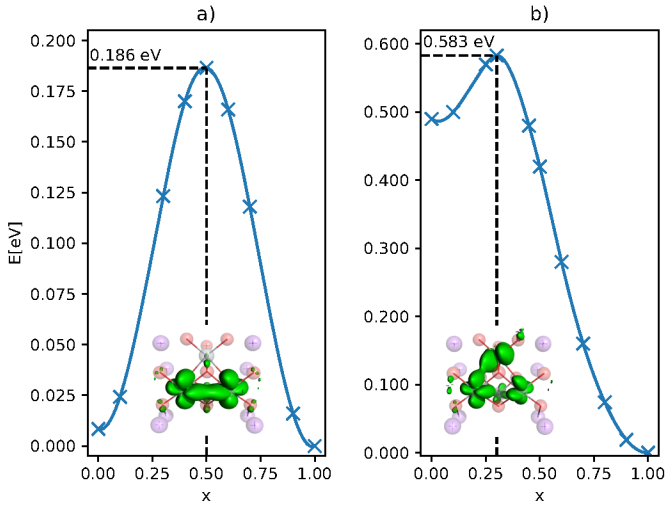

Figure 4: Calculated barrier profiles for the transition L3-7/L2-10 to L3-7/L2-9 (a) and L3-7/L1-3 to L3-7/L2-9 (b). In both plots x = 1.0 is equal to configuration L3-7/L2-9. The lowest lying configuration in energy serves as zero point for the energy scale. Also shown is the spin density of the corresponding transition state. Isosurface level 0.015 eÅ^{-3}.

Gaussian type orbital basis set[46]—employing a 2 × 2 × 1 k-point grid. Geometries have been relaxed until residual force fell below 10^{-2} eV/Å. A detailed description of the methodology used to estimate barriers is given in the supplementary material.

Acknowledgements

The authors would like to thank the German Research Foundation DFG (Grant OB425/4-1) and the Solar Technologies Go Hybrid Initiative of the State of Bavaria for support. Partially funded by the Deutsche Forschungsgemeinschaft (DFG, German Research Foundation) under Germany's Excellence Strategy EXC 2089/1 390776260.

Supporting Information

Supporting Information Available:

A detailed description of the used pristine and defected structural models and the methods

used to generate them. A full list of calculated polaron localization patterns. A discussion of the influence of the chosen U value on relative polaron stabilities. All simulation details of the presented barrier calculations, a discussion of the influence of the chosen U value on polaron hopping barrier heights, and the computational details for all calculations. Finally, a detailed description of the model used to determine the electronic conductivity.

References

(1) Islam, M. S.; Fisher, C. A. J. Lithium and sodium battery cathode materials: computational insights into voltage, diffusion and nanostructural properties. *Chem. Soc. Rev.* **2014**, *43*, 185–204.

(2) Zhao, B.; Ran, R.; Liu, M.; Shao, Z. A comprehensive review of $Li_4Ti_5O_{12}$-based electrodes for lithium-ion batteries: The latest advancements and future perspectives. *Mater. Sci. Eng. R Rep* **2015**, *98*, 1–71.

(3) Chu, S.; Majumdar, A. Opportunities and challenges for a sustainable energy future. *Nature* **2012**, *488*, 294 EP–.

(4) Armand, M.; Tarascon, J.-M. Building better batteries. *Nature* **2008**, *451*, 652 EP–.

(5) Aricò, A. S.; Bruce, P.; Scrosati, B.; Tarascon, J.-M.; van Schalkwijk, W. Nanostructured materials for advanced energy conversion and storage devices. *Nat. Mater.* **2005**, *4*, 366–377.

(6) Heenen, H. H.; Scheurer, C.; Reuter, K. Implications of occupational Disorder on ion mobility in $Li_4Ti_5O_{12}$ battery materials. *Nano Lett.* **2017**, *17*, 3884–3888.

(7) Yuan, T.; Yu, X.; Cai, R.; Zhou, Y.; Shao, Z. Synthesis of pristine and carbon-coated $Li_4Ti_5O_{12}$ and their low-temperature electrochemical performance. *J. Power Sources* **2010**, *195*, 4997–5004.

(8) Yan, B.; Li, M.; Li, X.; Bai, Z.; Yang, J.; Xiong, D.; Li, D. Novel understanding of carbothermal reduction enhancing electronic and ionic conductivity of $Li_4Ti_5O_{12}$ anode. *J. Mater. Chem. A* **2015**, *3*, 11773–11781.

(9) Qiu, J.; Lai, C.; Gray, E.; Li, S.; Qiu, S.; Strounina, E.; Sun, C.; Zhao, H.; Zhang, S. Blue hydrogenated lithium titanate as a high-rate anode material for lithium-ion batteries. *J. Mater. Chem. A* **2014**, *2*, 6353–6358.

(10) Kaftelen, H.; Tuncer, M.; Tu, S.; Repp, S.; Göçmez, H.; Thomann, R.; Weber, S.; Erdem, E. Mn-substituted spinel $Li_4Ti_5O_{12}$ materials studied by multifrequency EPR spectroscopy. *J. Mater. Chem. A* **2013**, *1*, 9973–9982.

(11) Jakes, P.; Granwehr, J.; Kungl, H.; Rüdiger-A, E. Mixed ionic-electronic conducting $Li_4Ti_5O_{12}$ as anode material for lithium ion batteries with enhanced rate capability - impact of oxygen non-stoichiometry and aliovalent Mg^{2+}-doping studied by electron paramagnetic resonance. *Z. Phys. Chem.* **2015**, *229*, 1439–1450.

(12) chun Tsai, P.; Nasara, R. N.; chen Shen, Y.; chao Liang, C.; wen Chang, Y.; Hsu, W.-D.; Tran, N. T. T.; kang Lin, S. Ab initio phase stability and electronic conductivity of the doped-Li4Ti5O12 anode for Li-ion batteries. *Acta Materialia* **2019**, *175*, 196 – 205.

(13) Nasara, R. N.; Tsai, P.-C.; Lin, S.-K. One-step synthesis of highly oxygen-deficient lithium titanate oxide with conformal amorphous carbon coating as anode material for lithium ion batteries. *Adv. Mater. Interfaces* **2017**, *4*.

(14) Cohen, A. J.; Mori-Sánchez, P.; Yang, W. Challenges for density functional theory. *Chem. Rev.* **2011**, *112*, 289–320.

(15) Deskins, N. A.; Rousseau, R.; Dupuis, M. Distribution of Ti^{3+} surface sites in reduced TiO_2. *J. Phys. Chem. C* **2011**, *115*, 7562–7572.

(16) Shibuya, T.; Yasuoka, K.; Mirbt, S.; Sanyal, B. A systematic study of polarons due to oxygen vacancy formation at the rutile TiO_2(110) surface by GGA+U and HSE06 methods. *J. Phys. Condens. Matter* **2012**, *24*, 435504.

(17) Setvin, M.; Franchini, C.; Hao, X.; Schmid, M.; Janotti, A.; Kaltak, M.; Van de Walle, C. G.; Kresse, G.; Diebold, U. Direct view at excess electrons in TiO_2 rutile and anatase. *Phys. Rev. Lett.* **2014**, *113*, 086402.

(18) Young, D.; Ransil, A.; Amin, R.; Li, Z.; Chiang, Y.-M. Electronic Conductivity in the $Li_{4/3}Ti_{5/3}O_4Li_{7/3}Ti_{5/3}O_4$ System and Variation with State-of-Charge as a Li Battery Anode. *Adv. Energy Mater.* **2013**, *3*, 1125–1129.

(19) Kick, M.; Reuter, K.; Oberhofer, H. Intricacies of DFT+U, not only in a numeric atom centered orbital framework. *J. Chem. Theor. Comput.* **2019**, *15*, 1705–1718.

(20) Reticcioli, M.; Setvin, M.; Schmid, M.; Diebold, U.; Franchini, C. Formation and dynamics of small polarons on the rutile TiO_2(110) surface. *Phys. Rev. B* **2018**, *98*, 045306.

(21) Kowalski, P. M.; Camellone, M. F.; Nair, N. N.; Meyer, B.; Marx, D. Charge localization dynamics induced by oxygen vacancies on the TiO_2(110) surface. *Phys. Rev. Lett.* **2010**, *105*, 146405.

(22) Deschanvres, A.; Raveau, B.; Sekkal, Z. Mise en evidence et etude cristallographique d'une nouvelle solution solide de type spinelle $Li_1 + xTi_2 - xO_4$ $0 \leq x \leq 0.333$. *Mater. Res. Bull.* **1971**, *6*, 699–704.

(23) Hohenberg, P.; Kohn, W. Inhomogeneous electron gas. *Phys. Rev.* **1964**, *136*, B864–B871.

(24) Perdew, J. P.; Burke, K.; Ernzerhof, M. Generalized gradient approximation made simple. *Phys. Rev. Lett.* **1996**, *77*, 3865–3868.

(25) Cohen, A. J.; Mori-Sánchez, P.; Yang, W. Insights into current limitations of density functional theory. *Science* **2008**, *321*, 792–794.

(26) Hubbard, J. Electron correlations in narrow energy bands. *Proc. R. Soc. A* **1963**, *276*, 238–257.

(27) Anisimov, V.; Zaanen, J.; Andersen, O. K. Band theory and Mott insulators: Hubbard U instead of Stoner I. *Phys. Rev. B* **1991**, *44*, 943–954.

(28) Dudarev, S. L.; Botton, G. A.; Savrasov, S. Y.; Humphreys, C. J.; Sutton, A. P. Electron-energy-loss spectra and the structural stability of nickel oxide: An LSDA+U study. *Phys. Rev. B* **1998**, *57*, 1505–1509.

(29) Dorado, B.; Amadon, B.; Freyss, M.; Bertolus, M. DFT + U. *Phys. Rev. B* **2009**, *79*, 235125.

(30) Allen, J. P.; Watson, G. W. Occupation matrix control of d- and f-electron localisations using DFT + U. *Phys. Chem. Chem. Phys.* **2014**, *16*, 21016–21031.

(31) Himmetoglu, B.; Floris, A.; de Gironcoli, S.; Cococcioni, M. "Hubbard-corrected DFT energy functionals: The LDA+U description of correlated systems". *Int. J. Quantum Chem.* **2014**, *114*, 14–49.

(32) Yim, C. M.; Pang, C. L.; Thornton, G. Oxygen vacancy origin of the surface band-gap state of TiO_2(110). *Phys. Rev. Lett.* **2010**, *104*, 036806.

(33) Diebold, U. The surface science of titanium dioxide. *Surf. Sci. Rep.* **2003**, *48*, 53–229.

(34) Moussa, J. E.; Schultz, P. A.; Chelikowsky, J. R. "Analysis of the Heyd-Scuseria-Ernzerhof density functional parameter space". *J. Chem. Phys* **2012**, *136*, 204117.

(35) Kohtani, S.; Kawashima, A.; Miyabe, H. Reactivity of trapped and accumulated electrons in titanium dioxide photocatalysis. *Catalysts* **2017**, *7*, 303.

(36) Morgan, B. J.; Watson, G. W. GGA+U description of lithium intercalation into anatase TiO_2. *Phys. Rev. B* **2010**, *82*, 144119.

(37) Oberhofer, H.; Reuter, K.; Blumberger, J. Charge Transport in Molecular Materials: An Assessment of Computational Methods. *Chem. Rev.* **2017**, *117*, 10319.

(38) Devreese, J. T. *digital Encyclopedia of Applied Physics*; American Cancer Society, 2003.

(39) Devreese, J.; on Fröhlich Polarons, A. S. I.; in Polar Semiconductors, E. P. I. *Polarons in Ionic Crystals and Polar Semiconductors*; NATO Advanced Study Institutes Series; North-Holland Publishing Company, 1972.

(40) Park, M.; Zhang, X.; Chung, M.; Less, G. B.; Sastry, A. M. A review of conduction phenomena in Li-ion batteries. *J. Power Sources* **2010**, *195*, 7904–7929.

(41) Wolfenstine, J.; Lee, U.; Allen, J. Electrical conductivity and rate-capability of $Li_4Ti_5O_{12}$ as a function of heat-treatment atmosphere. *J. Power Sources* **2006**, *154*, 287 – 289.

(42) Dutta, A. K. Electrical Conductivity of Single Crystals of Graphite. *Phys. Rev.* **1953**, *90*, 187–192.

(43) Creffield, G. K.; Down, M. G.; Pulham, R. J. Electrical resistivity of liquid and solid lithium. *J. Chem. Soc., Dalton Trans.* **1974**, 2325–2329.

(44) Stenina, I. A.; Il'in, A. B.; Yaroslavtsev, A. B. Synthesis and ionic conductivity of $Li_4Ti_5O_{12}$. *Inorg. Mater.* **2015**, *51*, 62–67.

(45) Blum, V.; Gehrke, R.; Hanke, F.; Havu, P.; Havu, V.; Ren, X.; Reuter, K.; Scheffler, M. Ab initio molecular simulations with numeric atom-centered orbitals. *Comput. Phys. Commun.* **2009**, *180*, 2175–2196.

(46) Lamiel-Garcia, O.; Ko, K. C.; Lee, J. Y.; Bromley, S. T.; Illas, F. When Anatase nanoparticles become bulklike: Properties of realistic TiO_2 nanoparticles in the 1–6 nm

size range from all electron relativistic density functional theory based calculations. *J. Chem. Theor. Comput.* **2017**, *13*, 1785–1793.

Graphical TOC Entry

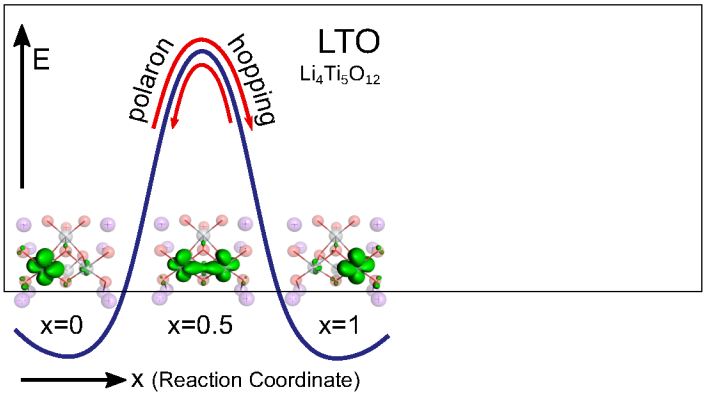

Energy profile for polaron hopping in LTO. The insets depict the polaron localization at different values of the reaction coordinate at the initial (x=0), transition (x=0.5), and final state (x=1).